Optimising A Compact Dual-Particle Imager with A Novel Combination of Organic and Inorganic Scintillators.

H. Al Hamrashdi[a*], S.D.Monk[b], D.Cheneler[b] and S. Al Mamari[a]

[a] Sultan Qaboos University, Muscat, Oman. hajir@squ.edu.om, s90188@student.squ.edu.om
[b] Lancaster University, Lancaster, UK. s.monk@lancaster.ac.uk, d.cheneler@lancaster.ac.uk

Abstract:

This work discusses the process of optimising the performance of a compact dual-particle imager with a fast response time of 60 s and a signal processing time of 60 s. The imaging concept relies on a radiation scattering technique with a neutron-scattering sub-system, a Compton-scattering sub-system and a thermal neutron absorption layer. The enhanced design proposed here reduces the signal processing time compared to earlier work. The time lagging occurs mainly during neutron-gamma discrimination within the neutron scattering sub-system. Hence, the optimisation here which mainly targets investigating two promising dual particle detectors EJ-212 and EJ-276D as possible replacement for the EJ-204 in the original device. The results indicated that EJ-212 and EJ-276D offer similar elastic scattering and escape probabilities of neutrons at energies less than 100 keV. At energies higher than 500 keV, the elastic scattering probabilities increase with thickness, reaching a maximum around 24% in both detectors. As for gamma-ray photons, the results showed that the two detectors have similar total mass attenuation coefficients. Further investigation showed that EJ-212 exhibits a higher Compton scattering cross-section with respect to EJ-276D. Additionally, results show that EJ-276D maintains the imager intrinsic efficiency while offering build-in neutron-gamma discrimination abilities.

Keywords: Neutrons; gamma photons; dual particles imagers, EJ-212 plastic scintillator, EJ-276D plastic scintillator.

1. Introduction

Localisation and characterisation of radiation sources and nuclear material is indispensable in many fields including, counterterrorism, borders security, nuclear industry, nuclear medicine, medical imaging and molecular imaging [1]. With the reported increase in the number of nuclear applications around the World, especially in the nuclear power industry, the need for fast, accurate and portable imaging systems that can localize radiation sources and nuclear material has become vital.

There are several imaging systems that offer accurate localisation and characterisation abilities in single mode radiation field emitters [1]. However, the type of radiation emitted varies across sources and nuclear materials and thus mixed field radiation detection has gained noticeable interest in recent years [1]. Sensitivity to both neutrons and gamma photons allows a wider range of radioactive sources and nuclear materials to be monitored and identified such as Special Nuclear Materials (SNM) and radiation protection applications [2][3][4]. Yet, a key challenge in radiation imaging is the development of a fast and accurate compact and portable imaging system that can efficiently detect and accurately identify the origin of highly penetrating neutrons and energetic gamma photons, both of which are emitted by SNM [1].

The main types of dual particle imager, as described in literature, are pixelated detectors, coded aperture imaging systems and multilayers scattering imaging systems [1]. Among these techniques, scatter imaging systems simultaneously offer the optimum combination of detection efficiency and special resolution, thus a wider application scope. Under this criterion, large imaging systems offer higher sensitivity and higher spatial resolution abilities, although applications are limited by their size [3] [4]. Other portable systems are restricted to passive fast neutron-gamma imaging systems where a collimated beam of radiation field from a well-defined source is targeted [5]. This technique limits target applications of the imager as well as its sensitivity since only radiation fields from a selected direction are allowed to reach the detection medium. Several dual-particle imagers offer portability and allow wider angular view such the CdZnTe based imager by M. Streicher et al. [6] the stilbene organic scintillators by Steinberger W. et al. [7] and the CLYC-6 imager by J. Lerendegui-Marco et al. [8]. For some of these systems, the energy range is confined.

The portable dual-particles imager system proposed in earlier work by the same authors was composed of three layers of detectors capable of imaging thermal neutrons, fast neutrons and gamma photons simultaneously [9]. With a scan time of 60s, the imager could locate radiation sources with a 15o angular resolution. While the system could analyse mixed radiation fields, longer processing time was required for PSD analysis of neutron-gamma events in the chosen

plastic scintillator, namely the EJ-204 [9]. That is because pulses from EJ-204 exhibit a very fast decay time, 1.8 nm, and very short a pulse width, 2.2 ns [9][10]. This can be mitigated by choosing a material featuring a longer decay time or inherently better neutron-gamma discrimination abilities.

Unlike many other types of detectors, plastic scintillators offer the flexibility of being tailored to a required shape or size, non-toxicity and non-flammability [11]. These features are highly desirable in a portable neutron-gamma imager. EJ-204 plastic scintillators have been already investigated for their ability to scatter fast neutron within dual particle imagers [9]. According to literature EJ-212 and EJ-276D can overcome the drawbacks in EJ-204 used in the fast neutron scattering sub-system [12][13][14][15]. EJ-212 offers similar features to EJ-204 with long optical attenuation length and an emission spectrum that matches most common photomultipliers. However, it has a longer decay time of 2.4 ns compared to EJ-204[16]. EJ-276D offers inherently superior neutron-gamma discrimination abilities due to it is long slow decay time, reportedly hundreds of nanoseconds [14] [15]. These features ensure that these two are a suitable replacement for the EJ-204 in the neutron scattering sub-system in the proposed novel compact dual-particle imager proposed in the earlier work by the author [9].

The objective of this current study is to study EJ-212 and EJ-276D, plastic scintillators for their abilities in attenuating fast neutrons and gamma photons at different energies. The results of this investigation will be used is means of enhancing the performance of the above mentioned dual-particle imager by replacing the plastic scintillator in the system. Additionally, the study aims to test the performance of the imager by calculating the intrinsic efficiency of the system using these two scintillators.

2. Materials and Methods

2.1 Imaging Concept.

The imaging concept of the system relies on radiation scattering techniques for both fast neutrons and gamma ray photons with a series of three layers of detectors separated by distances d_1 and d_2 as shown in Fig. 1.

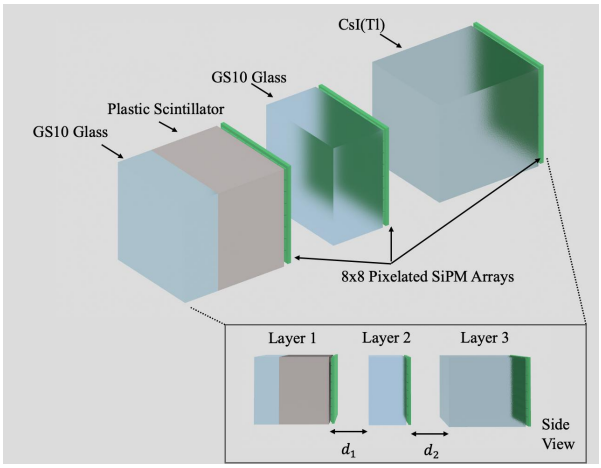

Fig. 1 A schematic of the imaging system consisting of four detectors arranged in three layers each layer backed with an 8x8 pixelated SiPM array. The three layers are arranged consecutively in a row joined by the same central axis. Layer one consists of

In the original study by H. Al Hamrashdi et al. [9] the analogy of the radiation imaging starts with a layer of a 10-mm Li-based glass detector (GS10) [17] combined via an optical gel with a 20-mm plastic scintillator (EJ-204) [12]. The role of the former is to capture thermal neutrons (neutrons with most probable energy of 0.025 eV) via $^{6}Li(n,\alpha)^{3}H$ thermal neutron capture reaction and the role of the latter is to scatter fast neutrons (neutrons with energies higher than 1 keV). Scattered neutrons will then interact in the GS10 glass detector in the second layer of the imaging system. Both layers are backed with high fill-factor J-series SiPM sensor array (ArrayJ-30035-64P- PCB 8 × 8 SiPM, SensL, Cork, Ireland [8]) used as the photodetector. The interaction of neutrons in this layer is mainly attributed to capture reactions. In this imaging system, a fast neutron undergoes elastic scattering whilst interacting with the protons within the plastic scintillator in the first layer followed by a capture (or inelastic scattering) in the glass scintillator in the second layer. The scattering angles and incident trajectories can be calculated from the relative positions of the detected pulses via the position of activated pixels in the SiPM array. The energy of an incident neutron is the sum of the energy of the

scattered proton, E_p, in the plastic scintillator and of the energy of the scattered neutron, E_n', that is detected in the second GS10 glass scintillator [30,31]. These energies are related to the scattering angle, ϑ, through eqn (1).:

$$\tan \vartheta^2 = \frac{E_p}{E_n'} \quad (1)$$

The energy of the scattered neutron can be calculated using the measurements of the time-of-flight (TOF) between the first and the second layers in seconds, as shown in eqn (2).

$$E_n' = \frac{1}{2} m_n \left(\frac{d}{TOF}\right)^2 \quad (2)$$

Where m_n is the mass of neutrons in kilograms and d is the distance in meters between the centre of the plastic scintillator in the first layer and the centre of the GS10 glass detector in the second layer. For every single neutron scattering event, the position of the scattering event is found from the pixelated SiPM, with a precision equal to the size of the pixel (3.07 × 3.07 mm^2), the energy of the scattered proton, the energy and the scattering angle of the fast neutrons will then be used to create a probability cone. The compound images of the probability cones (of the circular base of the cones) for all successful scattering events will give the location of the fast neutrons source. A schematic of the neutron imaging sub-system is given in Fig. 2.

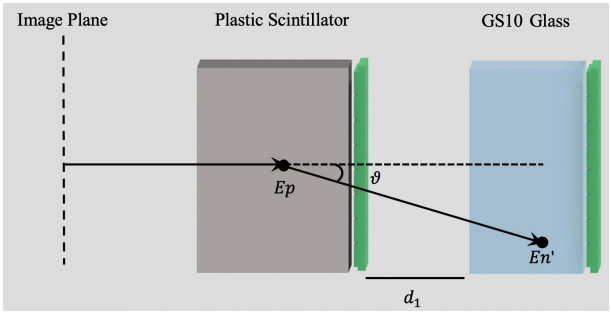

Fig. 2 Neutron scattering sub-system.

Gamma-ray sources are imaged using Compton scattering technique in the second and the third layers of the imaging system [18]. The design of the imaging system, particularly the design of the first layer, ensures that gamma photons will solely interact in the second and the third layers of the design. Incident gamma photons in the Compton energy range (∼10 keV–∼10 MeV) will undergo Compton scattering in the GS10 detector in the second layer. The location of the interaction position and the energy of the Compton electrons, E_e, will be registered via the pixelated SiPM array in this layer. Scattered gamma photons will then undergo the photoelectric effect in the CsI(Tl) detector in the third layer. The energy of the scattered photon, E_γ', will be registered via the pixelated SiPM array as shown in Fig. 3.

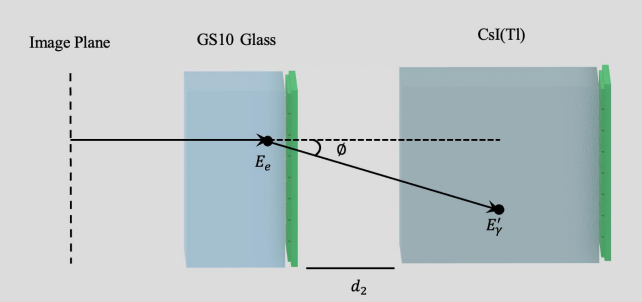

Fig. 3 Gamma Compton scattering sub-system.

Using the registered information in layers two and three, the scattering angle of the incident is calculated using the following equation:

$$cos\ \emptyset = 1 - m\ c^2\left(\left(\frac{1}{E'_\gamma}\right) - \left(\frac{1}{E'_\gamma - E_e}\right)\right) \quad (3)$$

where $m\ c^2$ is the rest mass of the electron in units of energy. For every Compton scattering event, a probability cone will be generated using the location of the pixel were the Compton scattering event was registered (cone's apex) and the scattering angle $\emptyset$ to create the base of the cone. The intersection of all cones generated by all successful Compton scattering events will be used to find the location of gamma-ray sources. The energy of incident gamma photons is found using the sum of the deposited Compton electron energy in layer two and the deposited energy of the scattered photon in layer three.

2.2 EJ-212 and EJ-276D Plastic Scintillators.

EJ-212 and EJ-276D scintillators share the same original base of a plastic matrix of polyvinyl toluene and fluors. The variation in this combination gives each scintillator it's unique properties. Both scintillators investigated in this study are from Eljen Technology's where EJ-212 is the equivalent to NE-102A and BC-400 commercial scintillators and EJ-276D is the equivalent to NE-142 and BC-452 commercial scintillators [12] [13]. The scintillation output of EJ-212 is 10,000 photons/MeV e- slightly higher than that for EJ-276D which is 8,000 photons/MeV e-. The maximum wavelength for these scintillation photons is around 423 nm for EJ-212 and 425 nm for EJ-276D. These two wavelengths coincide with the photon detection efficiency range of Onsemi SiPM J-series array [19] that is used in this imager as the photomultiplier. In terms of material density, EJ-212 has a slightly lower density compared to EJ-276D with a reported density of 1.023 for the former and 1.099 for the latter. When it comes to neutron interaction with detection material, it is the light nuclei content that greatly effects the interaction cross section. EJ-212 is composed of 8.5% Hydrogen and 91.5% Carbon, while EJ-276D is composed of 7.3% Hydrogen and 92.7% Carbon.

2.3 Means of comparison and calculations of interest

Optimising this instrument involves maximising the neutron elastic scattering abilities of the plastic scintillator, while minimising neutron absorption. The response of each detector was investigated at 10 varying thicknesses (10 mm, 20 mm, 30 mm, 40 mm, 50 mm, 60 mm, 80 mm, 100 mm, 150 mm, 250 mm) at 6 different energies: (1 keV, 10 keV, 100 keV, 0.5 MeV, 1 MeV and 5 MeV).Gamma photons attenuation was investigated at 8 different energies: (0.01 MeV, 0.025 MeV, 0.05 MeV, 0.1 MeV, 0.7 MeV, 1.0 MeV, 5 MeV and 10 MeV). This range of energies covers the range of possible gamma photon energies in radiation detection applications [1] . Total mass attenuation coefficient can be calculated using eqn. (4):

$$\mu_m = \mu/\rho = \lambda n\ (I/I_o) / x \quad (4)$$

Where μ is the linear attenuation coefficient, ρ is the mass density of the detector, I is the intensity of radiation after passing through thickness x of the material in hand and Io is the original intensity of the incident radiation field. To further investigate the two detectors for SNM non-proliferation applications, Compton scattering cross sections for the two detectors at 25 mm were found at 8 different energies. Lower Compton scattering probabilities will further verify the abilities of the detector to substitute EJ-204 in the neutron scattering sub-system. The overall performance of the imager was examined with the two candidate detectors. The intrinsic efficiency was calculated using a Cf-252 source.

The testing environment was simulated using Monte Carlo simulations in Geant4.11.1 simulation toolkit with room temperature (293 K) assumed throughout [20] . Cross section data for fast neutrons simulations are based on G4NDL

data libraries which is based on multiple libraries including ENDF/B-VII.0 and JENDL-4.0 [20]. Gamma simulations in Geant4 are based on Electromagnetic (EM) physics modelling. The model is based on the Livermore evaluated library [20]. The geometry of the detectors follows the same geometry as the EJ-204 detector described in section 2.1.

3. Results and discussion

3.1 EJ-212 and EJ-276D neutron attenuation abilities

The simulation results of single elastic scattering efficiency and escaping probability versus thickness for EJ-212 are illustrated in Fig. 4. The trend of elastic scattering probability as a function of thickness varies among this list of energies. At 5 MeV elastic scattering probability reaches a peak of 22 % of the total events at around 60 mm thickness before declining as this increases. The peak shifts to smaller thicknesses at 1 MeV and 0.5 MeV. At 100 keV, 10 keV and 1 keV the probabilities of elastic scattering decreases with increasing EJ-212 thickness. A common trend for all incident neutron energies in Fig. 4 is the exponential decay of the escaping probabilities as a function of thickness in EJ-212. However, the decrease in the escaping probability at energies 5 MeV, 1 MeV is less rapid compared to that at lower energies namely the 1 keV and the 10 keV energies. In general, for all energies the probability of elastic scattering is higher than the probability of escaping at thicknesses greater than 25 mm.

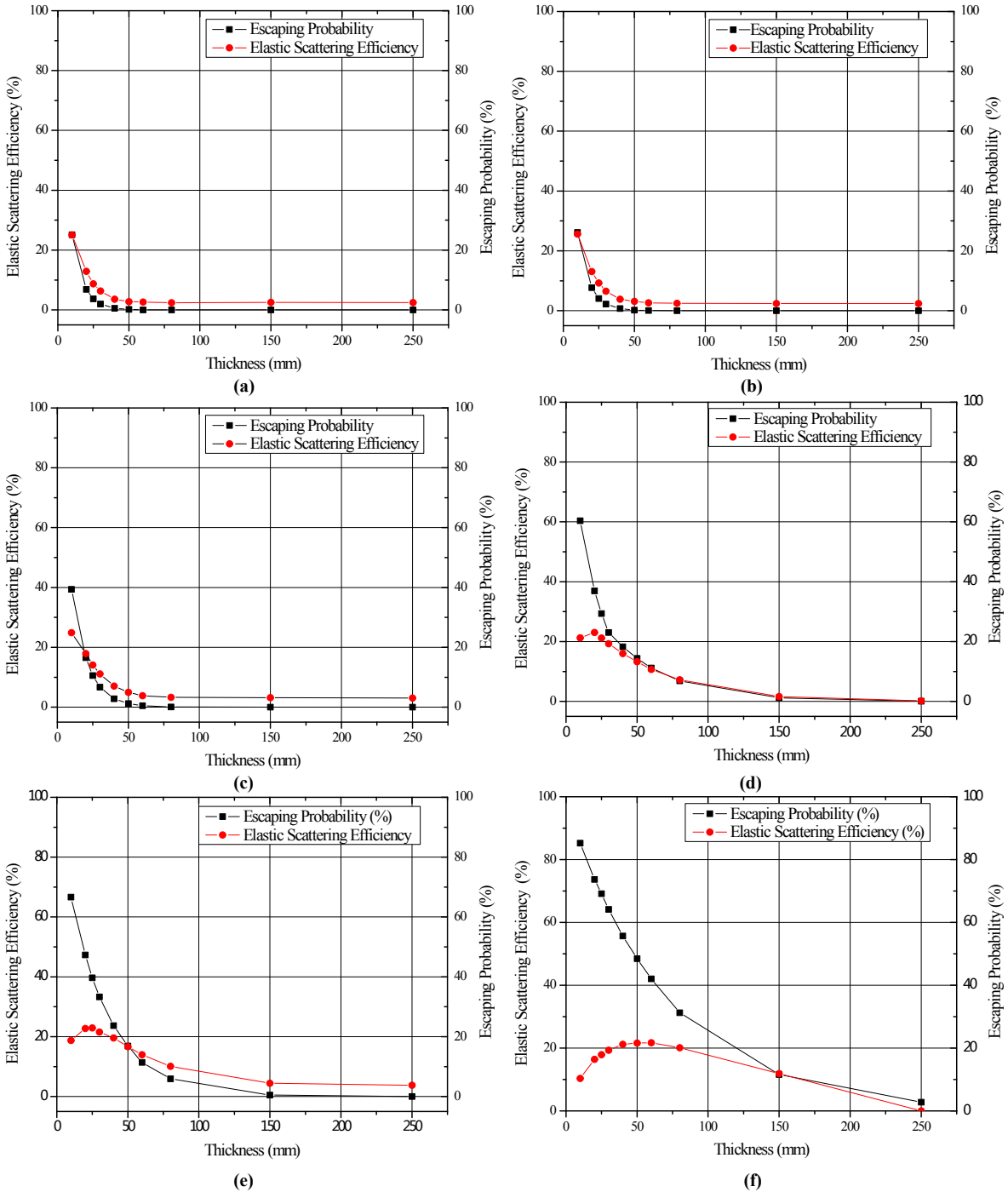

Fig. 4 Elastic scattering probability and escaping probability in EJ-212 at (a) 1 keV, (b) 10 keV, (c) 100 keV, (d) 0.5 MeV (e) 1 MeV and (f) 5 MeV.

Similarly, neutrons single elastic scattering probability and escaping probability in EJ-276D were investigated and the results are shown in Fig. 5. The trend of elastic scattering probability as a function of thickness varies among this list of energies with both probabilities decreasing as the thickness increases. At 5 MeV elastic scattering probability reaches a peak of at around 50 mm thickness before declining as the thickness increases. The peak shifts to smaller thicknesses at 1 MeV and 0.5 MeV. Like EJ-212, at lower energies as can be seen in Fig. 5 (a), (b) and (c), the probabilities of elastic scattering decreases with increasing EJ-276D thickness. A mutual trend for all incident neutron energies in Fig. 4 is the

exponential decay of the escaping probabilities as a function of thickness in EJ-276D. Like EJ-212, the decrease in the escaping probability at energies 5 MeV, 1 MeV and 0.5 MeV is less rapid compared to that at lower energies. Overall, at thicknesses greater than 25 mm and for all energies, the probability of elastic scattering is higher than the probability

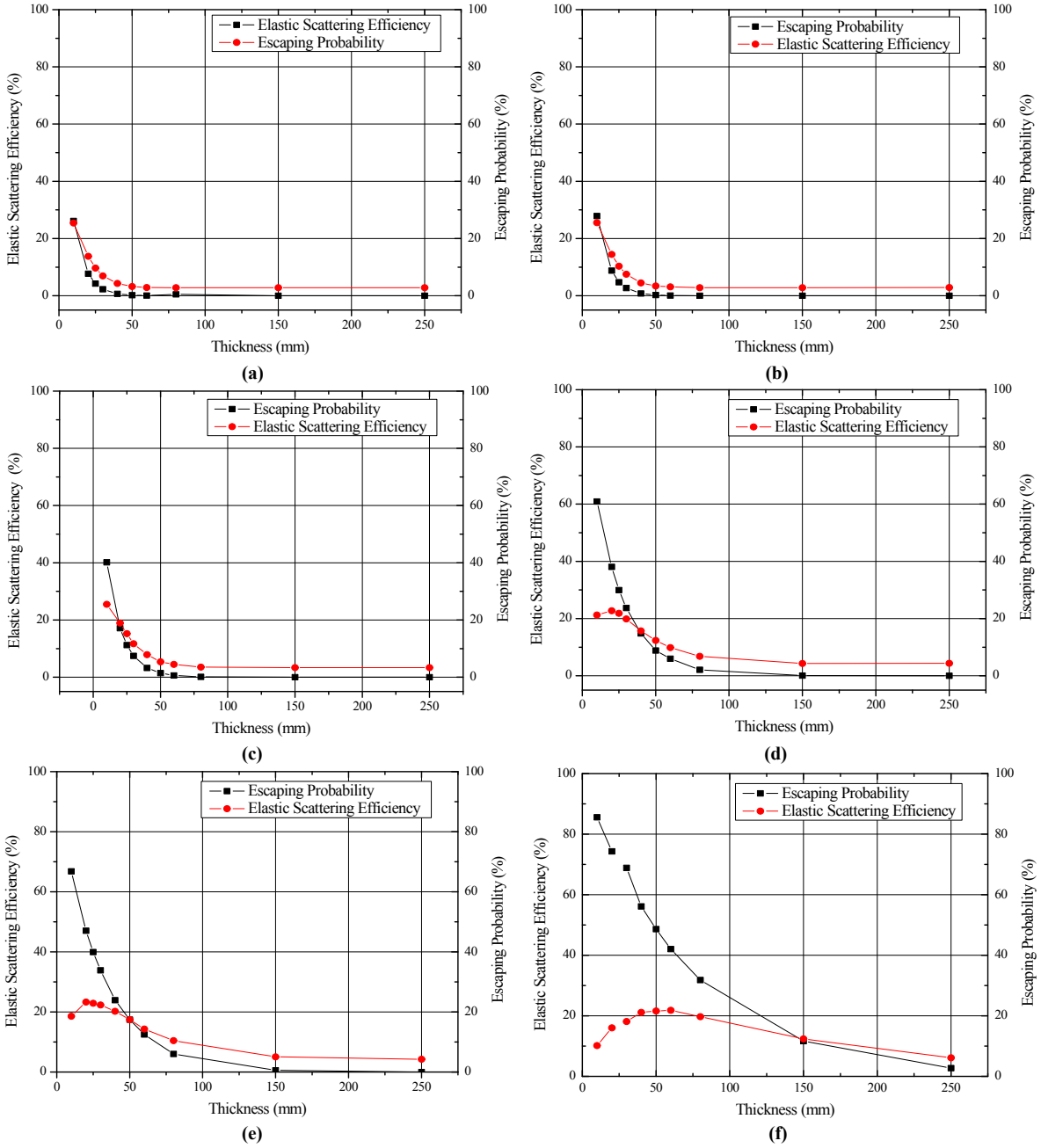

Fig. 5 Elastic scattering probability and escaping probability in EJ-276D at (a) 1 keV, (b) 10 keV, (c) 100 keV, (d) 0.5 MeV (e) 1 MeV and (f) 5 MeV.

of escaping. Overall, both detectors exhibit similar fast neutrons attenuation abilities.

3.2 EJ-212 and EJ-276D attenuation abilities of gamma photons

The total mass attenuation coefficients in the energy range between 0.01 MeV and 10 MeV were calculated using eqn(2) for both EJ-212 and EJ-276D. The results were compared to NIST values (extracted using XCOM database 3.1 [9]) at this energy range as shown in Fig. 6. The results show good agreement with the expected mass attenuation coefficient

values from NIST, with the mass attenuation coefficient decreasing with increasing gamma energy. Compared to the results

Fig. 6 Total mass attenuation coefficient as function of energy for EJ-212 plastic scintillator and EJ-276D.

given by H. Al Hamrashdi et. al [11], both detectors have similar mass attenuation coefficients as the widely used EJ-309 gamma-neutron detector, which reflects their ability to be used in gamma ray imaging.

To further investigate the abilities of the two detectors in being used in Compton scattering imaging systems, appropriate probabilities for each detector were studied as functions of incident energy as shown in Fig. 7 (with the thickness of the two plastic scintillators fixed at 25 mm). The figure shows that for both detectors the probability of Compton scattering increases between 0.01MeV and 0.05 MeV before it starts gradually declining beyond this energy. In general, EJ-212 showed higher Compton scattering abilities compared to EJ-276D, with highest percentage difference of 11.4 % recorded at the same location as the highest Compton scattering probability for both detectors at an energy of 0.05 MeV. This is attributed to the fact that the probability of Compton scattering decreases with the increase of energy beyond 0.05MeV [21]. Another relevant conclusion from the results here is that at any given thickness, EJ-276D causes less Compton scattering events compared to EJ-212, hence less gamma scattering events will occur within this detector in the neutron scattering sub-system in the dual particle imager.

Fig. 7 Compton scattering probability as function of energy for EJ-212 and EJ-276D plastic scintillators at 25 mm thickness.

3.3 Special case study: Testing new configuration of a dual particle imaging system with EJ-212 and EJ-276D.

EJ-212 and EJ-276D scintillators were investigated as potential replacements of EJ-204 in the dual portable particle neutron- gamma-scattering system proposed by H. Al Hamrashdi et. al. [9]. The imaging concept discussed in section 1.3 explained the neutron scattering imaging concept and how neutron detection happens within the system. Using Cf-252 with an average energy of 2.1 MeV as a neutron source, the intrinsic efficiency in that system was found to be 6.1 × 10−3. In this work, the simulations were repeated using the same neutron source, but with different scattering layers. The intrinsic efficiency of the system using EJ-212 was found to be 5.9×10-3 , whereas the intrinsic efficiency of the system using EJ-276D is 6.1×10-3. Compared to the reported value with by H. Al Hamrashdi et. al. [9], EJ-276D scored the fast neutrons intrinsic efficiency as EJ-204, whereas EJ-212 scored slightly lower efficiency. Based on the results above, EJ-276D offers advantageous features and therefore is currently the most appropriate candidate to EJ-204 detector in the dual particle imaging system.

4. Conclusions

Within this study, the performance of a hybrid portable dual particle imager was enhanced by investigating two plastic scintillators, namely EJ-212 and EJ-276D, as neutron scattering layers within its neutron scattering subsystem. The two candidates were tested for their neutron attenuation abilities and gamma attenuation abilities using a wide range of energies. The overall intrinsic efficiency of the system with the two scintillators was investigated using Monte Carlo simulations with Cf-252 as a fast neutron source. The results indicated that both detectors share similar fast neutron scattering efficiencies. These results agree with the measurements of fast neutrons intrinsic efficiency of the system using the two detectors. The intrinsic efficiency of EJ-276D was found to be in the order of 6.1×10-3, whereas the intrinsic efficiency of EJ-212 was found to be in the order of 5.9×10-3. Compared to EJ-204 detectors, EJ-276D maintains the imagers fast neutrons detection efficiency while EJ-212 exhibits lower fast neutrons detection efficiency. These results along with the reported built-in PSD abilities of EJ-276D show that the detector is the best replacement for EJ-204, and it will enhance the original processing time of the imager while maintaining its computationally and experimentally reported efficiencies.

Author contributions

H. Al Hamrashdi designed this work, contributed to the simulation, did the analysis and wrote the initial draft. S. D. Monk and D. Cheneler participated in originating ideas and reviewing the draft. S. Al Ma'Amari worked on simulations.

Conflicts of interest

The authors declare no competing interests.

Data availability

All datasets generated or analysed during this study are available from the corresponding author upon reasonable request.

Acknowledgements

The This work was financially supported by Sultan Qaboos University under Internal Grant IG/SCI/PHYS/22/03.

References

[1] H. Al Hamrashdi, S. D. Monk, and D. Cheneler, "Passive gamma-ray and neutron imaging systems for national security and nuclear non-proliferation in controlled and uncontrolled detection areas: Review of past and current status," Jun. 01, 2019, MDPI AG. doi: 10.3390/s19112638.

[2] IAEA, “IAEA Safegaurdig ,” 2011.
[3] P. B. Rose, A. S. Erickson, M. Mayer, J. Nattress, and I. Jovanovic, “Uncovering Special Nuclear Materials by Low-energy Nuclear Reaction Imaging,” Sci Rep, vol. 6, Apr. 2016, doi: 10.1038/srep24388.
[4] A. Poitrasson-Rivière et al., “Angular-resolution and material-characterization measurements for a dual-particle imaging system with mixed-oxide fuel,” Nucl Instrum Methods Phys Res A, vol. 797, pp. 278–284, Oct. 2015, doi: 10.1016/j.nima.2015.06.045.
[5] J. Shuai et al., “Experimental study of plastic scintillators array for compact fast neutron-gamma dual-modality imaging system,” Nucl Instrum Methods Phys Res A, vol. 1064, Jul. 2024, doi: 10.1016/j.nima.2024.169485.
[6] M. Streicher, S. Brown, Y. Zhu, D. Goodman, and Z. He, “Special Nuclear Material Characterization Using Digital 3-D Position Sensitive CdZnTe Detectors and High Purity Germanium Spectrometers,” IEEE Trans Nucl Sci, vol. 63, no. 5, pp. 2649–2656, 2016, doi: 10.1109/TNS.2016.2593631.
[7] R. Lopez, W. M. Steinberger, N. Giha, P. Marleau, S. D. Clarke, and S. A. Pozzi, “Neutron and gamma imaging using an organic glass scintillator handheld dual particle imager,” Nucl Instrum Methods Phys Res A, vol. 1042, Nov. 2022, doi: 10.1016/j.nima.2022.167407.
[8] J. Lerendegui-Marco et al., “Simultaneous Gamma-Neutron Vision device: a portable and versatile tool for nuclear inspections,” EPJ Tech Instrum, vol. 11, no. 1, Feb. 2024, doi: 10.1140/epjti/s40485-024-00108-w.
[9] H. Al Hamrashdi, D. Cheneler, and S. D. Monk, “A fast and portable imager for neutron and gamma emitting radionuclides,” Nucl Instrum Methods Phys Res A, vol. 953, Feb. 2020, doi: 10.1016/j.nima.2019.163253.
[10] D. P. Broughton et al., “Commissioning a time-gated camera for fast neutron beamline spatial-energy characterization at LANSCE-WNR spallation source,” Nucl Instrum Methods Phys Res A, vol. 1071, Feb. 2025, doi: 10.1016/j.nima.2024.170088.
[11] H. Al Hamrashdi, D. Cheneler, and S. D. Monk, “Material optimization in dual particle detectors by comparing advanced scintillating materials using two Monte Carlo codes,” Nucl Instrum Methods Phys Res A, vol. 869, pp. 163–171, Oct. 2017, doi: 10.1016/j.nima.2017.06.043.
[12] “GENERAL PURPOSE EJ-200, EJ-204, EJ-208, EJ-212.”
[13] “PULSE SHAPE DISCRIMINATION EJ-276D & EJ-276G.”
[14] F. Pino et al., “Novel Detector Assembly for Neutron/Gamma-Ray Discrimination Applications Based on Large-Sized Scintillators Coupled to Large Area SiPM Arrays,” IEEE Trans Nucl Sci, vol. 69, no. 4, pp. 668–676, Apr. 2022, doi: 10.1109/TNS.2022.3154015.
[15] M. Grodzicka-Kobylka et al., “Fast neutron and gamma ray pulse shape discrimination in EJ-276 and EJ-276G plastic scintillators,” Journal of Instrumentation, vol. 15, no. 3, Mar. 2020, doi: 10.1088/1748-0221/15/03/P03030.
[16] I. Holl, E. Lorenz, and G. Mageras, “A measurement of the light yield of common inorganic scintillators,” IEEE Trans Nucl Sci, vol. 35, no. 1, pp. 105–109, 1988, doi: 10.1109/23.12684.
[17] “Lithium-6 glass scintillators for neutron detection.”
[18] D. B. Everett, J. S. Fleming, R. W. Todd, and J. M. Nightingale, “Gamma-radiation imaging system based on the Compton effect,” Proceedings of the Institution of Electrical Engineers, vol. 124, no. 11, p. 995, 1977, doi: 10.1049/piee.1977.0203.
[19] “Silicon Photomultipliers (SiPM) | ARRAYJ.” Accessed: Feb. 20, 2025. [Online]. Available: https://www.onsemi.com/products/sensors/photodetectors-sipm-spad/silicon-photomultipliers-sipm/arrayj
[20] J. Allison et al., “Geant4 developments and applications,” IEEE Trans Nucl Sci, vol. 53, no. 1, pp. 270–278, 2006, doi: 10.1109/TNS.2006.869826.
[21] M. J. Berger et al., “XCOM: Photon Cross Sections Database.”